Eur. Phys. J. B **62**, 171–177 (2008)
DOI: 10.1140/epjb/e2008-00132-y

THE EUROPEAN PHYSICAL JOURNAL B

Chaos out of internal noise in the collective dynamics of diffusively coupled cells

M. Gosak[a], M. Marhl, and M. Perc

Department of Physics, Faculty of Natural Sciences and Mathematics, University of Maribor, Koroška cesta 160, 2000 Maribor, Slovenia

Received 19 September 2007 / Received in final form 12 February 2008
Published online 2 April 2008 –

Abstract. We study the transition from stochasticity to determinism in calcium oscillations via diffusive coupling of individual cells that are modeled by stochastic simulations of the governing reaction-diffusion equations. As expected, the stochastic solutions gradually converge to their deterministic limit as the number of coupled cells increases. Remarkably however, although the strict deterministic limit dictates a fully periodic behavior, the stochastic solution remains chaotic even for large numbers of coupled cells if the system is set close to an inherently chaotic regime. On the other hand, the lack of proximity to a chaotic regime leads to an expected convergence to the fully periodic behavior, thus suggesting that near-chaotic states are presently a crucial predisposition for the observation of noise-induced chaos. Our results suggest that chaos may exist in real biological systems due to intrinsic fluctuations and uncertainties characterizing their functioning on small scales.

PACS. 05.40.-a Fluctuation phenomena, random processes, noise, and Brownian motion – 05.45.-a Nonlinear dynamics and chaos – 05.45.Tp Time series analysis – 87.16.Ac Theory and modeling; computer simulation

1 Introduction

Mathematical modeling is commonly used when studying the behavior and properties of biological systems. Traditionally, the temporal behavior of a system is thereby described by a set of ordinary differential equations. This deterministic approach assumes that the temporal evolution of a reacting system is a continuous process, which is acceptable only if the number of molecules, participating in forming the solution, is large enough. In systems, where molecule numbers are rather small, however, it is required to simulate the temporal development of a reacting system by stochastic algorithms. In general, realistic biological systems, especially at the cellular but partially also tissue level, where volumes and particle concentrations are indeed low, require the slightly more sophisticated stochastic approach.

It is a well-established fact that intracellular calcium is one of the most important second messengers in the cytosol of living cells [1,2]. In a large variety of cell types, calcium oscillations regulate and define many crucial processes, ranging from muscle contractions and fertilization to cell death [3]. Almost from the outset of calcium oscillation investigations, experiments have been accompanied by mathematical modeling. Since the number of membrane receptors, ion channels, and calcium ions in some organelles is very low, stochastic effects cannot always be neglected. Therefore the stochastic modeling of intracellular calcium signaling pathways has recently gained a remarkable attention [2,4–8]. Several different aspects of calcium signaling in various types of cells have been recognized to require a stochastic treatment. Stochastic models have been developed for the modeling of single calcium channels [6,9], intracellular calcium oscillations [7,10], and for the intracellular calcium wave propagation [4,5]. In addition, coherence and stochastic resonance phenomena on the temporal [11–13] and spatial [14] scale as well as the transition from stochasticity to determinism [5,8,15] has been investigated.

Several techniques have been proposed and developed in order to take into account influences of stochastic effects, ranging from additive noisy perturbations of system parameters or variables to conventional birth-death processes governed by master equations [16]. As an alternative, Monte Carlo procedures for the numerical simulation of reacting systems have also been developed (for review see [17]), and their implications in various systems have turned out to be immense.

It is a widespread and extremely well documented fact that noise can dramatically influence the system's dynamics. Consequently, the impact of noise on different dynamical systems presents a mushrooming field of research. Although numerous studies have been reported

[a] e-mail: marko.gosak@uni-mb.si

that are related with the role of fluctuations in dynamical systems, in the present paper we are focused on noise-induced chaos. The phenomenon was first observed in a driven nonlinear oscillator by Crutchfield et al. [18], and after that studied via the noisy logistic map [19] and biochemical systems [20]. Later on, several reports have been performed about the noise-inducement of chaos in systems, which are deterministically in a non-chaotic regime [21–26].

In the present paper we extend above findings and show that internal stochastic effects, determining and regulating cellular dynamics, are able to induce chaos in the collective behavior of diffusively coupled cells if the bifurcation parameter is set proximately to chaotic behavior in bifurcation diagram. As expected, for large ensemble sizes the stochastic solutions seem to gradually converge to their deterministic limit, but we find, that in case of periodic deterministic limits the stochastic collective solutions are periodic only if the system is not near a chaotic state. Otherwise, internal fluctuations induce chaos, although the number of coupled cells is large, so that the determinism in not disputable. We confirm our finding by calculating the return map, the normalized autocorrelation function and the maximal Lyapunov exponent. The results are discussed in context of possible explanation of chaotic behavior usually observed experimentally in recordings of real-life functioning of whole organs.

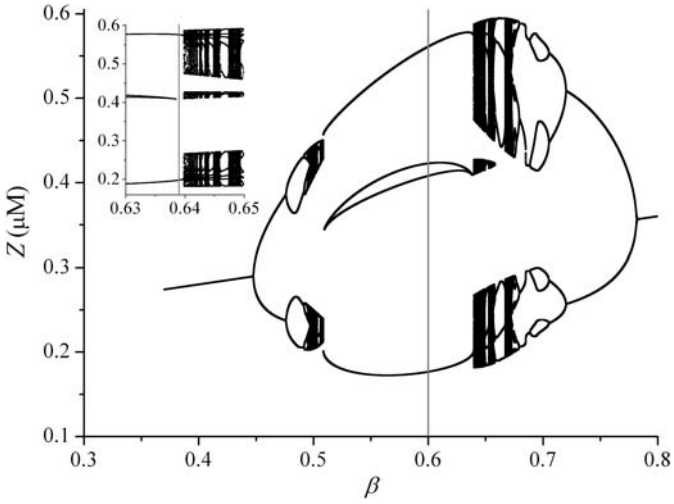

Fig. 1. Bifurcation diagram for cytosolic calcium in a single cell. Grey lines indicate parameter values used in our calculations. In the inset it can be noticed that in one case the system is set close to the chaotic regime ($\beta = 0.639$). Importantly, this bifurcation diagram has been shown already in [27], whereas here we show it for completeness and basic introduction of the employed model. System parameters are: $K_2 = 0.1$ μM, $K_5 = 0.3194$ μM, $K_A = 0.1$ μM, $K_d = 1.0$ μM, $K_Y = 0.3$ μM, $K_Z = 0.6$ μM, $k = 10.0$ s^{-1}, $k_f = 1.0$ s^{-1}, $\varepsilon = 11.0$ s^{-1}, $n = 4$, $m = 2$, $p = 1$, $V_0 = 2.0$ μM s^{-1}, $V_1 = 2.0$ μM s^{-1}, $V_{M2} = 6.0$ μM s^{-1}, $V_{M3} = 30.0$ μM s^{-1}, $V_{M4} = 3.0$ μM s^{-1}, $V_{M5} = 50.0$ μM s^{-1}.

2 Calcium dynamics of coupled cells

The mathematical model used to describe the temporal dynamics of Ca^{2+} is determined by theoretical framework of Houart et al. [27]. Specifically, the model considers changes of free Ca^{2+} concentration in the cytosol (Z), in the intracellular calcium store (Y), as well as the dynamics of IP_3 (A). Here, the model equations are presented only briefly (for a detailed description see [27]). The free Ca^{2+} concentrations in the cytosol, in the intracellular calcium store and the concentration of IP_3 are calculated by the following differential equations (the parameter values used in our calculations are quoted in the caption of Fig. 1):

$$\frac{dZ}{dt} = V_{in} - V_2 + V_3 + k_f Y - kZ, \tag{1}$$

$$\frac{dY}{dt} = V_2 - V_3 - k_f Y, \tag{2}$$

$$\frac{dA}{dt} = \beta V_4 - V_5 - \varepsilon A, \tag{3}$$

where

$$V_{in} = V_0 + \beta V_1, \tag{4}$$

$$V_2 = V_{M2}\frac{Z^2}{K_2^2 + Z^2}, \tag{5}$$

$$V_3 = V_{M3}\frac{Z^m}{K_Z^m + Z^m}\frac{Y^2}{K_y^2 + Y^2}\frac{A^4}{K_A^4 + A^4}, \tag{6}$$

$$V_5 = V_{M5}\frac{A^p}{K_5^p + A^p}\frac{Z^n}{K_d^n + Z^n}. \tag{7}$$

The spatial extension of the model is devised so that individual cells are arranged on a square lattice with periodic boundary conditions. The coupling is modeled by introducing an additional diffusive flux of the form $D\nabla^2 Z_{i,j}$ to the differential equation describing changes of cytosolic calcium concentration $Z_{i,j}$ (Eq. (1)) in each of the coupled cells on the $L \times L$ ($i, j \in [1, L]$) square lattice, whereby D is the diffusion coefficient. In the lattice, the cell corresponding to $Z_{i,j}$ has four neighbors located to the north, south, east and west with concentrations $Z_{i+1,j}$, $Z_{i-1,j}$, $Z_{i,j+1}$ and $Z_{i,j-1}$, respectively. When the diffusion process is approximated by the first-order transport reaction rate, we have $D\nabla^2 Z_{i,j} \approx D(Z_{i+1,j} + Z_{i-1,j} + Z_{i,j+1} + Z_{i,j-1} - 4Z_{i,j})/\Delta\delta^2$, where $\Delta\delta$ represents the spacing between nearest-neighbor cells. For simplicity we define the junctional coupling coefficient as $\gamma = D/\Delta\delta^2$, using $\gamma = 20$ s^{-1} in all below calculations. Although IP_3 is also an important messenger in intercellular communication, for simplicity and without loss of generality, in our calculations diffusive coupling via IP_3 is not considered.

To simulate the system stochastically, we used Gillespie's τ-leap method [28], which is an approximation of the exact stochastic simulation method [29], but is computationally less expensive. Importantly, since we are dealing with differential equations, the stochastic simulation is employed similarly as exemplified by Gracheva et al. [5] or Li et al. [12], where reaction rates are ascribed to fluxes, constituting the differential equations. These reaction rates determine, through a Poissonian distribution,

Table 1. Reaction rates and corresponding stochastic processes entailed in a given iteration of the employed τ-leap algorithm. Note that $\Omega = N_A V$.

Reaction rate	Stochastic process
$r_1 = \Omega V_{\text{in}}$	$Z_{i,j} \to Z_{i,j} + k_1/\Omega$
$r_2 = \Omega V_2$	$Z_{i,j} \to Z_{i,j} - k_2/\Omega, \quad Y_{i,j} \to Y_{i,j} + k_2/\Omega$
$r_3 = \Omega V_3$	$Z_{i,j} \to Z_{i,j} + k_3/\Omega, \quad Y_{i,j} \to Y_{i,j} - k_3/\Omega$
$r_4 = \Omega k_f Y$	$Z_{i,j} \to Z_{i,j} + k_4/\Omega, \quad Y_{i,j} \to Y_{i,j} - k_4/\Omega$
$r_5 = \Omega k Z$	$Z_{i,j} \to Z_{i,j} - k_5/\Omega$
$r_6 = \Omega \beta V_4$	$A_{i,j} \to A_{i,j} + k_6/\Omega$
$r_7 = \Omega V_5$	$A_{i,j} \to A_{i,j} - k_7/\Omega$
$r_8 = \Omega \varepsilon A$	$A_{i,j} \to A_{i,j} - k_8/\Omega$
$r_9 = \Omega D \lvert Z_{i+1,j} - Z_{i,j} \rvert$	$Z_{i,j} \to Z_{i,j} + k_9/\Omega,\ Z_{i+1,j} \to Z_{i+1,j} - k_9/\Omega$ for $Z_{i+1,j} - Z_{i,j} > 0$ $Z_{i,j} \to Z_{i,j} - k_9/\Omega,\ Z_{i+1,j} \to Z_{i+1,j} + k_9/\Omega$ for $Z_{i+1,j} - Z_{i,j} < 0$
$r_{10} = \Omega D \lvert Z_{i-1,j} - Z_{i,j} \rvert$	$Z_{i,j} \to Z_{i,j} + k_{10}/\Omega,\ Z_{i-1,j} \to Z_{i-1,j} - k_{10}/\Omega$ for $Z_{i-1,j} - Z_{i,j} > 0$ $Z_{i,j} \to Z_{i,j} - k_{10}/\Omega,\ Z_{i-1,j} \to Z_{i-1,j} + k_{10}/\Omega$ for $Z_{i-1,j} - Z_{i,j} < 0$
$r_{11} = \Omega D \lvert Z_{i,j+1} - Z_{i,j} \rvert$	$Z_{i,j} \to Z_{i,j} + k_{11}/\Omega,\ Z_{i,j+1} \to Z_{i,j+1} - k_{11}/\Omega$ for $Z_{i,j+1} - Z_{i,j} > 0$ $Z_{i,j} \to Z_{i,j} - k_{11}/\Omega,\ Z_{i,j+1} \to Z_{i,j+1} + k_{11}/\Omega$ for $Z_{i,j+1} - Z_{i,j} < 0$
$r_{12} = \Omega D \lvert Z_{i,j-1} - Z_{i,j} \rvert$	$Z_{i,j} \to Z_{i,j} + k_{12}/\Omega,\ Z_{i,j-1} \to Z_{i,j-1} - k_{12}/\Omega$ for $Z_{i,j-1} - Z_{i,j} > 0$ $Z_{i,j} \to Z_{i,j} - k_{12}/\Omega,\ Z_{i,j-1} \to Z_{i,j-1} + k_{12}/\Omega$ for $Z_{i,j-1} - Z_{i,j} < 0$

how much the values of Z, Y and A will increase or decrease in a given time interval τ. Importantly, this is a crucial step in accommodating the Gillespie's stochastic simulation, initially intended for chemical reaction schemes, so that it can be formulated on the basis of a differential equation. In accordance with the fluxes, a discrete change of particular concentration of the form $k_x/(N_A V)$ is performed at each iteration, where N_A is the Avogadro's number, V is the volume of each coupled cell and k_x is an integer, obtained from the Poissonian

$$P(r_x, \tau) = \frac{e^{-r_x \tau} (r_x \tau)^{k_x}}{k_x!}, \tag{8}$$

where r_x ($x = 1...12$) are reaction rates of all possible stochastic processes. In Table 1 a description of those rates and the corresponding processes is presented. During a time interval τ, each of the twelve reaction rates is evaluated and the related stochastic process is executed as dictated by k_x obtained from equation (8).

Importantly, V directly determines the level of internal fluctuations, which are best expressed by low particle numbers and vanish in the thermodynamic limit given by $V \to \infty$. Since concentrations Z, Y, and A are of the same order of magnitude, the number of particles depends directly on the volume of the corresponding compartment. The smallest volume appearing in the model represents the intracellular calcium store, of which the volume is around $V = 30\ \mu\text{m}^3$. According to the relation between the concentration (c) and the number of particles (N) given by $c = N/(N_A V)$, and for the aforementioned volume V, the number of particles by the simulation in each compartment varies between 3×10^3 and 10^4. In this case, the signal of each individual cell is substantially burdened and blurred by the impact of stochasticity, as discussed already in [8].

3 Results

First, we demonstrate in Figure 1 the bifurcation diagram showing minima and maxima of cytosolic calcium concentration (Z) in a single cell. The model equations (Eqs. (1–3)) were integrated numerically with fixed parameter values listed in the caption of Figure 1, whereas the level of stimulation β was taken as the bifurcation parameter. Noteworthy, the model exhibits a rich dynamical behavior explored accurately already within [27], whereas for our analyses we focus on two dynamical states in particular; namely on $\beta = 0.60$ yielding periodic oscillations, and on $\beta = 0.639$ also yielding periodic behavior, but importantly, such that is in immediate parametrical proximity to an abrupt transition to chaos appearing at $\beta = 0.6398$. Although in the continuation we will mainly focus on the dynamics of coupled cells ($L > 1$), the bifurcation diagram for the single cell presented in Figure 1 provides insights into the dynamics of the most basic structure of the model, and as such is representative also of the coupled system. In particular, although the bifurcation diagram, and especially the specific bifurcation points, may shift in dependence on L and D, these changes are minute and insignificant for the parameters used within the present work (see also Fig. 6).

We observe the collective dynamics of the ensemble of cells, which is approximated via a simple mean-field approximation given by $(z, y, a) = (1/L \times L) \sum_{i=1}^{L \times L} (Z_i, Y_i, A_i)$. Evidently, the total amount of coupled cells is varied via

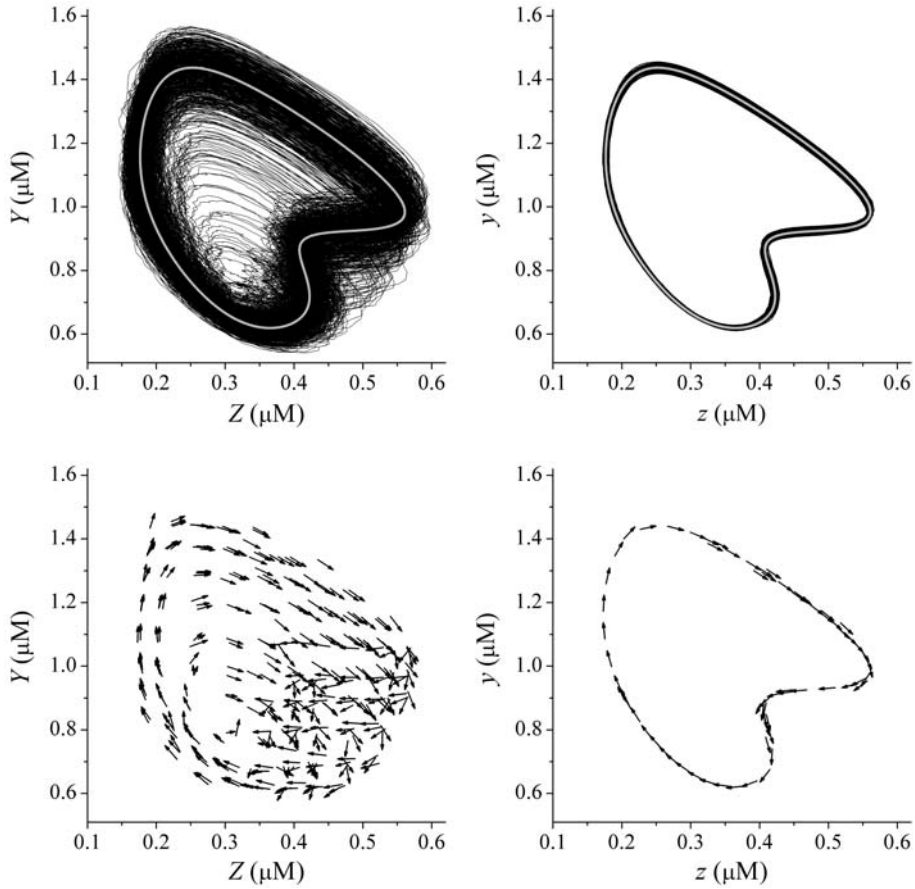

Fig. 2. Phase space plots (top row) obtained via stochastic integration (black line), and the pertaining average directional vector field approximations (bottom row) for one cell (left column) and the collective dynamics of 10×10 cells (right column) for $\beta = 0.60$. The gray line in phase space plots indicates the deterministic solution of the system obtained via the conventional Runge-Kutta numerical integration procedure.

the parameter L. Perc et al. [8] have shown that signals become increasingly noise free and smooth, i.e. deterministic, as the number of coupled cells increases. We can substantiate this in Figures 2 ($\beta = 0.60$) and 3 ($\beta = 0.639$), where phase space portraits for a single cell (upper left panel) and for the group of 10×10 cells (upper right panel) are featured. While the single cell signal obviously yields an erratic and non-smooth solution in the phase space, the signal of the mean field of coupled cells is remarkably noise-free and smooth.

To determine the level of stochasticity in the system, we use the method originally proposed by Kaplan and Glass [30], which is based on measuring average directional vectors in a coarse-grained phase space. The idea is that, in case of a deterministic solution, neighboring trajectories in a small portion of the phase space should all point in the same direction, i.e. not cross, thus assuring uniqueness of solutions, which is the hallmark of determinism. The determinism factor $0 \leq \kappa \leq 1$ is obtained by calculating the average length of all resultant vectors pertaining to a particular phase space box, whereby the resultant vectors are obtained by assigning a unit vector to each pass of the trajectory through a particular phase space box and calculating their vector sum. Hence, if the dynamics of oscillations is deterministic, the average length of all directional vectors κ will be 1, while for a completely random system $\kappa = 0$. Lower two panels of Figures 2 and 3 display directional vector fields for the corresponding phase space plots shown in the upper two panels. Figure 4 features results of the determinism test for different L. It is obvious that with the increasing number of coupled cells $\kappa \to 1$.

However, by considering results presented in Figures 2 – 4 more precisely, another fascinating feature can be observed. It is obvious that although for $L \geq 8$ the solutions are essentially deterministic ($\kappa > 0.98$) for both bifurcation parameter values, on the one hand, the solution for $\beta = 0.60$ evidently approaches the deterministic limit, but on the other hand, the solution for $\beta = 0.639$ fails to settle onto the limit cycle attractor, which characterizes the deterministic solution. In fact, these solutions in the phase space remarkably resemble chaotic attractors. In order to confirm this, we calculate the return maps, the normalized autocorrelation functions and the maximal Lyapunov exponents for the solution of 10×10 cells for both bifurcation parameter values.

In Figure 5 (left panel) the return map is presented, where the main successive maxima of cytosolic calcium

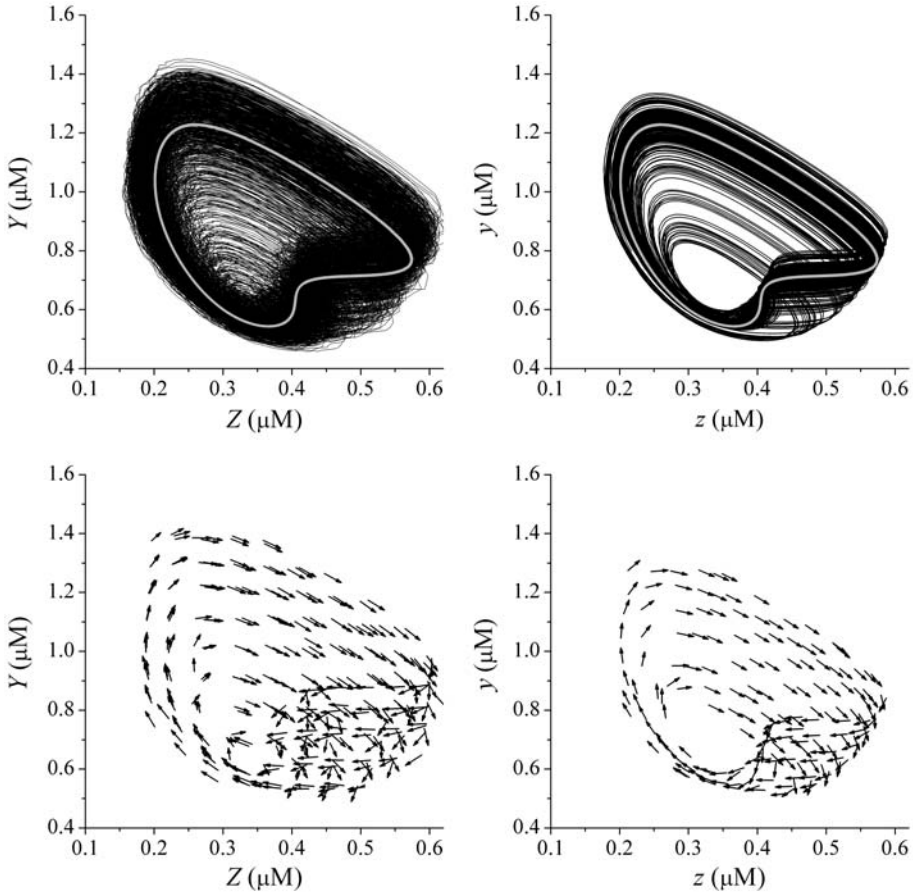

Fig. 3. Phase space plots (top row) obtained via stochastic integration (black line), and the pertaining average directional vector field approximations (bottom row) for one cell (left column) and the collective dynamics of 10×10 cells (right column) for $\beta = 0.639$. The gray line in phase space plots indicates the deterministic solution.

concentration are plotted against their predecessors. It can nicely be noted that for $\beta = 0.60$ the maximums are localized around a fixed point and for $\beta = 0.639$ they form an almost continuous curve, which evidences chaotic behavior.

In order to quantify the temporal order of Ca^{2+} oscillations we also compute the normalized autocorrelation function

$$C(\tau) = \frac{\langle \tilde{z}_t \tilde{z}_{t+\tau} \rangle}{\langle \tilde{z}^2 \rangle}, \tag{9}$$

where $\tilde{z} = z - \langle z \rangle$. We can observe in the middle panel of Figure 5 that for the bifurcation parameter value set deeply within the periodic regime the amplitude of undulations of $C(\tau)$ remains virtually unchanged, but in case the bifurcation parameter is set close to the chaotic regime this amplitude decreases continuously. Since both analyzed traces are exposed to the same amount of stochasticity (see Fig. 4), the obvious difference in the decay of the two autocorrelation functions can be ascribed only to the qualitative difference in their dynamics. Accordingly, we conclude that by $\beta = 0.60$ the trace is periodic, whereas by $\beta = 0.639$ the apparent decay of the autocorrelation function clearly evidences chaotic behavior.

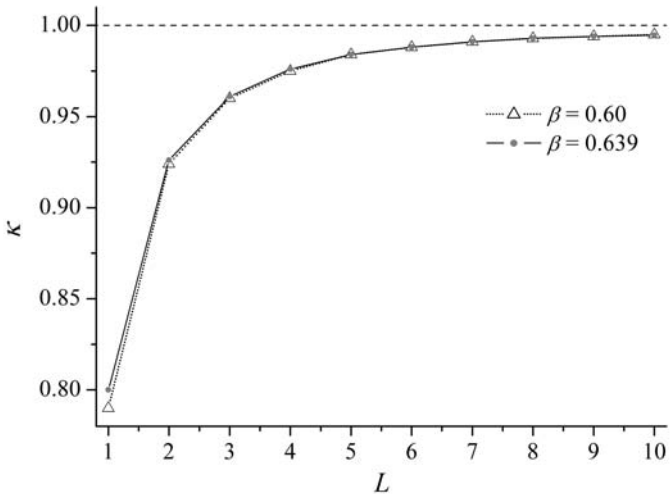

Fig. 4. Determinism factor of phase space solutions (z, y, a) obtained by different L for $\beta = 0.60$ and $\beta = 0.639$.

Finally, the maximal Lyapunov exponent λ_{max} is calculated by using the algorithm proposed by Wolf et al. [31]. Note that, since the phase space solution was obtained via Monte Carlo simulations, we employ the

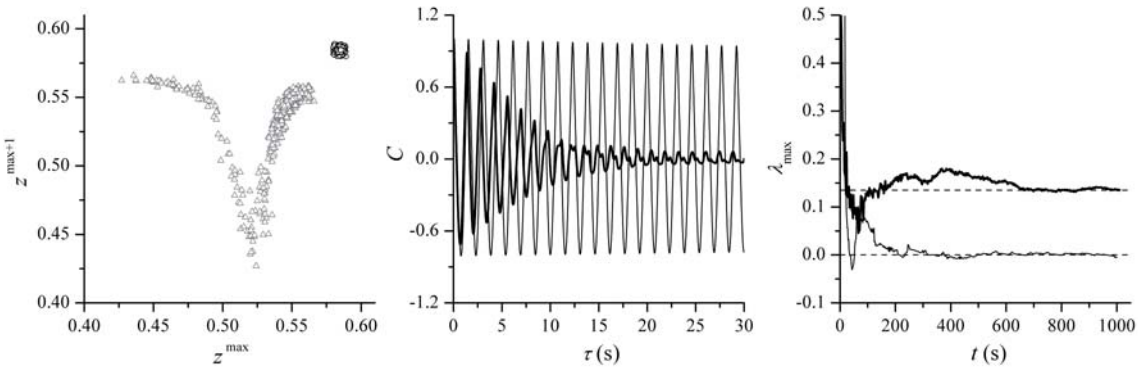

Fig. 5. Return map ($\beta = 0.60$ black circles; $\beta = 0.639$ gray triangles), autocorrelation function ($\beta = 0.60$ thin line; $\beta = 0.639$ thick line), and the convergence of the maximal Lyapunov exponent for the phase space solutions (z, y, a) obtained by 10×10 coupled cells ($\beta = 0.60$ thin line; $\beta = 0.639$ thick line).

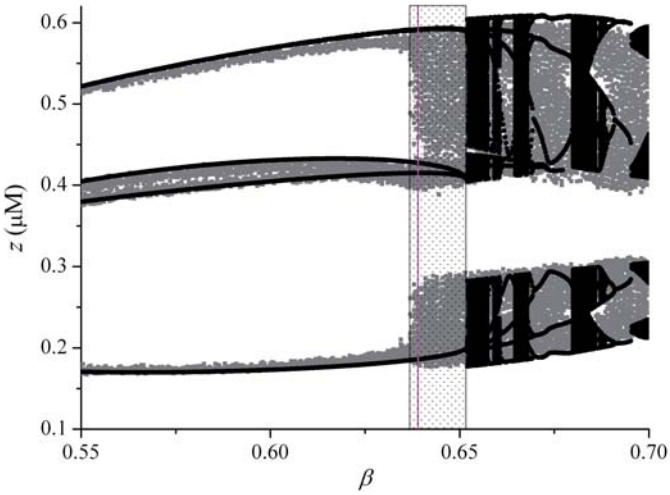

Fig. 6. Bifurcation diagram for coupled cells ($L = 10$). Black circles indicate minima and maxima of z obtained via deterministic integration, whereas gray squares were obtained by using the stochastic integration procedure. The marked area represents the region of internal-noise induced chaos, as determined more rigorously in Figure 5 for $\beta = 0.639$ (pink line).

algorithm developed in the framework of nonlinear time series [32], only that presently the original phase space given by the set of variables (z, y, a), instead of the reconstructed phase space from a single observed quantity is used. In Figure 5 (right panel) the maximal Lyapunov exponent for both bifurcation parameter values is shown. We can observe, that it converges very convincingly to a positive value $\lambda_{max} \approx 0.14\ \mathrm{s}^{-1}$ for $\beta = 0.639$, while the value for $\beta = 0.60$ is zero.

Our calculations reveal that internal noise can induce chaos in the collective dynamics of diffusively coupled cells in case the bifurcation parameter is set sufficiently close to the deterministically chaotic regime. Thus, we argue that internal noise is able to anticipate the abrupt bifurcation leading to chaos. In order to confirm this reasoning conclusively, we show in Figure 6 an insert of the bifurcation diagram for the collective dynamics of cytosolic calcium for 10×10 coupled cells. Although the coupling slightly shifts the deterministic occurrence of chaos towards higher values of β (compared to single cell dynamics; see Fig. 1), the value of $\beta = 0.639$ is still sufficiently close to the deterministically chaotic regime for internal noise to anticipate it. It can be observed nicely that the bifurcation diagram for coupled cells obtained via the stochastic integration procedure (gray squares) differs substantially from that obtained via deterministic integration (black circles), but only within the region close to the bifurcation leading to chaos, whereas outside the marked area changes are limited to small-amplitude fluctuations of min/max values of z. While the bifurcation diagram obtained via the stochastic integration procedure itself could not be considered a stringent test for noise-induced chaos, it nevertheless provides conclusive evidences for the mechanism behind the observed phenomenon, and together with the preceding thorough analysis presented in Figures 4 and 5, allows us to conclude that internal noise is able to induce chaos in the collective dynamics of diffusively coupled cells via a premature inducement of an abrupt transition to chaos occurring within the fully deterministic model.

4 Discussion

We study the transition from stochastic to deterministic behavior in the collective dynamics of diffusively coupled cells. While the stochastic simulation of a single cell at physiologically relevant conditions, whether uncoupled or coupled with its neighbors, exhibits a largely stochastic oscillatory behavior with well-expressed baseline and peak height fluctuations, these stochastic effects vanish in the collective dynamics of diffusively coupled cells for large enough ensembles. Remarkably, if the bifurcation parameter places the system close to chaotic behavior, the stochastic solution does not settle onto the limit cycle attractor even for large ensembles, despite the fact that (for coupled or individual cells) the deterministic integration procedure yields fully periodic behavior. An abrupt transition to chaos is a necessary precondition to observe this phenomenon; meaning it cannot be observed for bifurcation parameter values placing the system in the midst of

periodic behavior. Namely, when the distance from the bifurcation to chaos is too large, internal stochasticity is not capable of prematurely anticipating the bifurcation and induce chaos (see Fig. 6). The abrupt transition to chaos directly postulates the ability to place the system close to the chaotic behavior, and thus warrants the necessary closeness to the bifurcation. This set-up, however, may not be possible in case of the period doubling route to chaos due to the many intermediate cascades, unless we initially put the system deeply into the period doubling regime (i.e. close to chaos; see [19]). Similar conclusions, indicating that larger noise intensities are required when the distance from chaos increases, were also obtained for the Lorenz system where the authors observed noise induced chaos out of a stable fixed point [25].

Most remarkably, this is still true for very high numbers of coupled cells that are comparable with numbers of cells in a small part of tissue, by which the collective solution is smooth and deterministic, yet not identical with the deterministic limit, which suggests that the physiologically omnipresent stochastic disturbances at the cellular level might be responsible for chaotic behavior usually observed experimentally in recordings of real-life functioning of whole organs. Namely, it is known that real-life experimental recordings of cellular functions often yield stochastically burdened traces [3,33], which we have also confirmed presently by our theoretical calculations. On the other hand, recordings of physiological functions at the organic level are often not only deterministic in appearance, but also chaotic, which has been confirmed mathematically several times for ECGs [34,35], human locomotion [36], mammal vocalization [37] and human respiration [38]. Our theoretical results suggest that the chaotic behavior may originate from proximity to special bifurcation points and the ubiquitous stochastic disturbances at the cellular level, which vanish at large scales.

Matjaž Perc acknowledges support from the Slovenian Research Agency (grant Z1-9629).

References

1. S. Schuster, M. Marhl, T. Höfer, Eur. J. Biochem. **269**, 1333 (2002)
2. M. Falcke, Advances in Phys. **53**, 255 (2004)
3. K.S.R. Cuthbertson, P.H. Cobbold, Nature **316**, 541 (1985)
4. M. Kraus, B. Wolf, B. Wolf, Cell Calcium **19**, 461 (1996)
5. M.E. Gracheva, R. Toral, J.D. Gunton, J. Theor. Biol. **212**, 111 (2001)
6. F.M. Gabhann, M.T. Yang, A.S. Popel, Biochem. Biophys. Acta **1746**, 95 (2005)
7. K. Prank, M. Waring, U. Ahlvers, A. Bader, E. Penner, M. Möller, G. Barbant, C. Schöfl, Syst. Biol. **2**, 31 (2005)
8. M. Perc, M. Gosak, M. Marhl, Chem. Phys. Lett. **421**, 106 (2006)
9. J.W. Shuai, P. Jung, Phys. Rev. Lett. **88**, 068102 (2002)
10. M. Kraus, B. Wolf, Naturwissenschaften **79**, 289 (1992)
11. S. Zhong, F. Qi, H. Xin, Chem. Phys. Lett. **342**, 583 (2001)
12. H. Li, Z. Hou, H. Xin, Phys. Rev. E **71**, 061916 (2005)
13. C.L. Zhu, Y. Jia, Q. Liu, L.J. Yang, X. Zhan, Biophys. Chem. **125**, 201 (2007)
14. M. Perc, M. Gosak, M. Marhl, Chem. Phys. Lett. **437**, 143 (2007)
15. U. Kummer, B. Krajnc, J. Pahle, A.K. Green, C.J. Dixon, M. Marhl, Biophys. J. **89**, 1603 (2005)
16. N.G. van Kampen, *Stochastic processes in physics and chemistry*, 2nd edn. (Elsevier, Amsterdam, 1992)
17. T.C. Meng, S. Somani, P. Dhar, In silico Biol. **4**, 24 (2004)
18. J.P. Crutchfield, B.A. Huberman, Phys. Lett. A **77**, 407 (1980)
19. J.P. Crutchfield, J.D. Farmer, B.A. Huberman, Phys. Rep. **92**, 45 (1982)
20. H. Herzel, W. Ebeling, Th. Schulmeister, Zeitschr. Naturf. **42a**, 136 (1987)
21. D.D. Dixon, J. Phys. A: Math. Gen. **28**, 5539 (1995)
22. J.B. Gao, S.K. Hwang, J.M. Liu, Phys. Rev. Lett. **82**, 1132 (1999)
23. S.K. Hwang, J.B. Gao, J.M. Liu, Phys. Rev. E **61**, 5162 (2000)
24. Z. Liu, Y.-C. Lai, L. Billings, I.B. Schwartz, Phys. Rev. Lett. **88**, 124101 (2002)
25. J.B. Gao, W.-W. Tung, N. Rao, Phys. Rev. Lett. **89**, 254101 (2002)
26. C. Gan, Nonlin. Dynam. **45**, 305 (2006)
27. G. Houart, G. Dupont, A. Goldbeter, Bull. Math. Biol. **61**, 507 (1999)
28. D.T. Gillespie, J. Chem. Phys. **115**, 1716 (2001)
29. D.T. Gillespie, J. Comp. Phys. **22**, 403 (1976)
30. D.T. Kaplan, L. Glass, Phys. Rev. Lett. **68**, 427 (1992)
31. A. Wolf, J.B. Swift, H.L. Swinney, J.A. Vastano, Physica D **16**, 285 (1985)
32. H. Kantz, T. Schreiber, *Nonlinear time series analysis* (Cambridge University Press, Cambridge, 1997)
33. T. Tordjmann, B. Berthon, M. Claret, L. Combettes, EMBO J. **16**, 5398 (1997)
34. M. Perc, Eur. J. Phys. **26**, 757 (2005)
35. T. Jagrič, M. Marhl, D. Štajer, Š.T. Kocjančič, T. Jagrič, M. Podbregar, M. Perc, Translational Research **149**, 145 (2007)
36. M. Perc, Eur. J. Phys. **26**, 525 (2005)
37. I. Wilden, H. Herzel, G. Peters, G. Tembrock, Bioacoustics: Int. J. Animal Sound and its Recording **9**, 171 (1998)
38. G.C. Donaldson, Respir. Physiol. **88**, 313 (1992)